Journal Pre-proofs

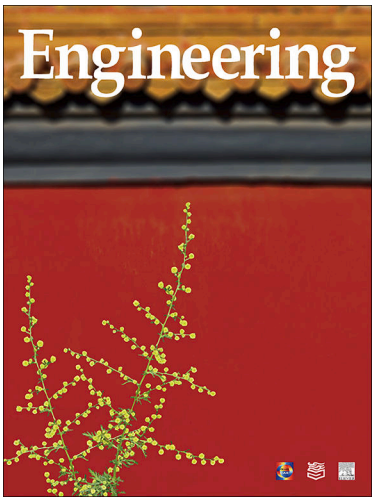

Article

A Novel Approach for Atomic-Scale Manufacturing via Enzymatic Hydrolysis Machining

Bing Wu, Yongjie Zhang, Yinhui Wang, Yongyu Fan, Rongyan Sun, Hui Deng

PII: S2095-8099(26)00073-1
DOI: https://doi.org/10.1016/j.eng.2026.01.024
Reference: ENG 2250

To appear in: *Engineering*

Received Date: 4 July 2025
Revised Date: 3 January 2026
Accepted Date: 15 January 2026

Please cite this article as: B. Wu, Y. Zhang, Y. Wang, Y. Fan, R. Sun, H. Deng, A Novel Approach for Atomic-Scale Manufacturing via Enzymatic Hydrolysis Machining, *Engineering* (2026), doi: https://doi.org/10.1016/j.eng.2026.01.024

This is a PDF of an article that has undergone enhancements after acceptance, such as the addition of a cover page and metadata, and formatting for readability. This version will undergo additional copyediting, typesetting and review before it is published in its final form. As such, this version is no longer the Accepted Manuscript, but it is not yet the definitive Version of Record; we are providing this early version to give early visibility of the article. Please note that Elsevier's sharing policy for the Published Journal Article applies to this version, see: https://www.elsevier.com/about/policies-and-standards/sharing#4-published-journal-article. Please also note that, during the production process, errors may be discovered which could affect the content, and all legal disclaimers that apply to the journal pertain.

© 2026 THE AUTHORS. Published by Elsevier LTD on behalf of Chinese Academy of Engineering and Higher Education Press Limited Company

Journal Pre-proofs

Research

Frontiers of Extreme Manufacturing—Article

A Novel Approach for Atomic-Scale Manufacturing via Enzymatic Hydrolysis Machining

Bing Wu [a], Yongjie Zhang [a], Yinhui Wang [a], Yongyu Fan [a], Rongyan Sun [b], Hui Deng [a,*]

[a] *Department of Mechanical and Energy Engineering, Southern University of Science and Technology, Shenzhen 518055, China*

[b] *Research Center for Precision Engineering, Graduate School of Engineering, The University of Osaka, Osaka 565-0871, Japan*

* Corresponding author.

E-mail address: dengh@sustech.edu.cn (H. Deng).

Graphical abstract

Journal Pre-proofs

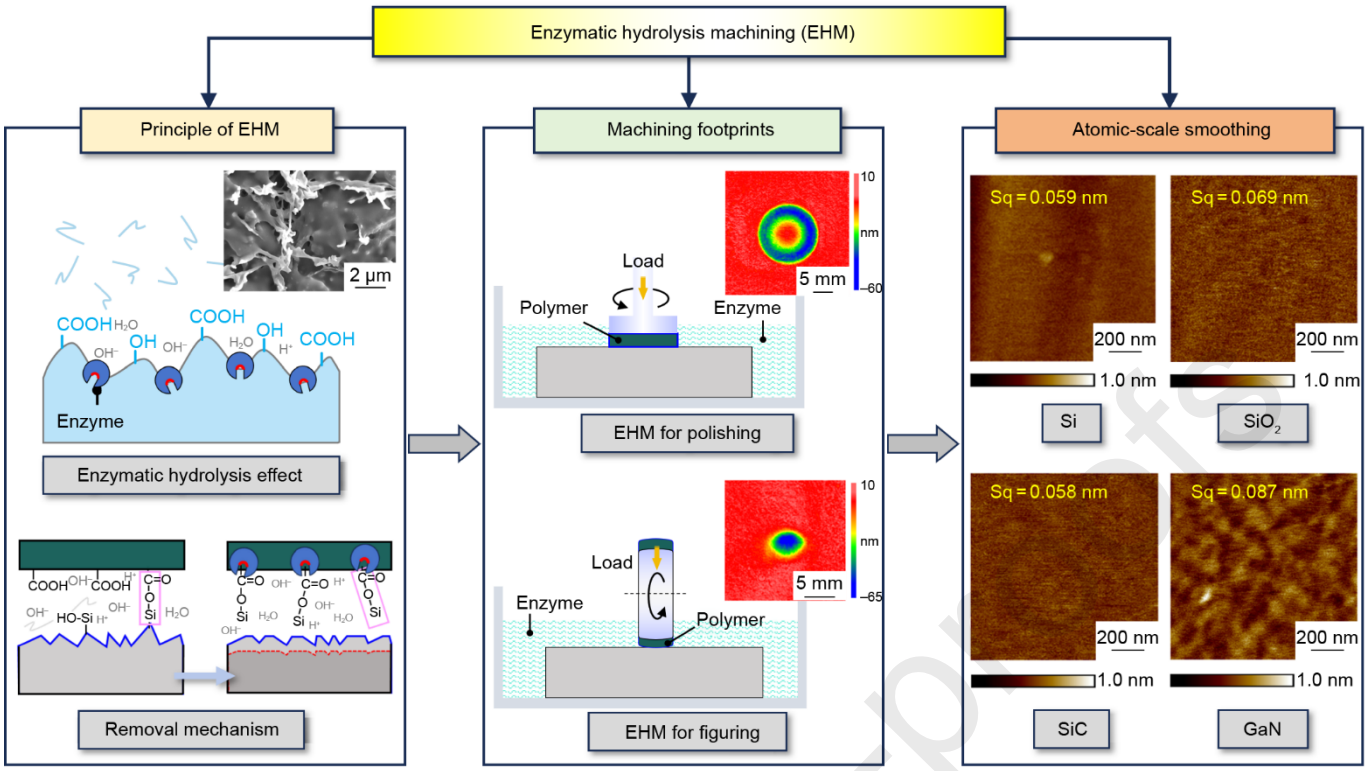

Abstract: Optics, semiconductors, and quantum technologies require atomic-scale manufacturing capabilities. However, the challenge lies in discovering or applying phenomena distinct from conventional macroscopic processes to realize atomic-scale and damage-free material removal. By employing biological enzymatic hydrolysis, an atomic-scale and abrasive-free machining technique, enzymatic hydrolysis machining (EHM), is proposed. Enzymatic hydrolysis regenerates abundant hydroxyl groups on the polymer surface, enabling the atomic-scale removal of Si through C–O–Si bridging bond formation and shearing. Static incubation experiments confirm the enzymatic hydrolysis effect, with hole/crack formation and carbonyl intensity reduction directly verifying ester bond scission. The removal depth of Si using polybutylene succinate (PBS) in pure water was 16.4 nm after 12 h, whereas it increased to 213.5 nm when *Humicola insolens cutinase* (HiC) was used. Pad-type and wheel-type tools obtain W-shaped and Gaussian-like removal functions for polishing and figuring, respectively. The volume removal rate was 3.8 × 10^{-5} $mm^3 \cdot min^{-1}$. EHM effectively achieved an atomically smooth Si surface (Sq = 0.05 nm, 5 μm × 5 μm viewing area). The generality of EHM is demonstrated by extending it to other materials (SiO_2, 4H-SiC, and GaN). Furthermore, numerically controlled EHM was applied to a 100 mm × 50 mm Si mirror, achieving a uniform atomically smooth surface across the entire area. This work shows that EHM is a novel and effective technique for atomic-scale manufacturing.

Keywords: Atomic-scale machining; Ezymatic hydrolysis; Polymers; Polishing; Figuring

1. Introduction

Progress in extreme ultraviolet (EUV), X-ray, and neutron optics demands optical components with increasingly stringent surface specifications [1,2]. Rayleigh's quarter-wavelength ($\lambda/4$) rule dictates that wavefront aberrations exceeding $\lambda/4$ compromise optical performance [1]. Given the short wavelength characteristics of EUV, X-ray, and neutron radiation, surface figure accuracy requirements for these components are demanding, reaching subnanometer accuracy. Moreover, surface roughness critically affects mirror reflectivity [3]. For instance, current synchrotron X-ray reflective mirrors typically require root-mean-square (RMS; Sq) roughness values below 0.3 nm [4]. Advanced beamlines even demand sub-0.1 nm Sq roughness. Consequently, achieving atomic-level precision across the entire spatial frequency is now imperative for X-ray mirror surface accuracy. Such stringent demands highlight the need for atomic-scale fabrication capabilities. Optics, semiconductors, and quantum technologies all rely heavily on advanced machining methods [5].

Machining is typically performed to create a controlled surface. Ideally, it produces geometrically and crystallographically perfect surfaces. Machining accuracy is determined by the minimum achievable material removal, which depends on the underlying phenomena employed [6]. Atomic-scale machining requires physical or chemical reactions to occur at the atomic level. This is different from the traditional macroscopic removal method based on plastic deformation and brittle fracture [7,8].

Current primary ultraprecision machining technologies include physical-based ion beam figuring (IBF) and chemical-based elastic emission machining (EEM) for EUV and X-ray optics [9,10]. IBF is a highly deterministic machining process. The physical sputtering effect achieves material removal at the atomic scale [11,12]. The energetic ions bombard and transfer energy to the surface atoms. When atoms gain adequate energy to conquer its binding energy, they escape from the top surface. Sigmund's theory demonstrated that material removal is related to the energy deposition area, which is Gaussian distributed [13]. This physical atomic-level removal capability can effectively correct the surface error of long spatial wavelengths. Zeiss Corporation (Germany) achieved 0.13 nm RMS figure accuracy for 178 mm-diameter spherical mirrors using IBF [9]. Wang et al. [4] developed an ion beam equipment for figuring of reflective X-ray mirrors. The slope error was reduced to 0.15 μrad and form error was reduced to 0.36 nm RMS. Nevertheless, IBF cannot optimize the surface microroughness during figuring, which requires ultrasmooth technology iteration. On the other hand, high-energy ion bombardment may introduce subsurface damage such as amorphous layers and dislocations.

EEM relies on the chemical interaction of fine powder with the substrate surface [6,14]. Both SiO_2 particles and Si substrate surfaces are capable of adsorbing hydroxyl groups in an aqueous environment. A Si–O–Si bridge bond is formed because of a dehydration reaction, and Si atoms are removed under fluid shearing [15]. These chemical reactions serve to remove tiny increments of the workpiece surface at the atomic scale. Thus, EEM does not introduce any crystallographic damage. In figuring, EEM is controllable over removal depths of 0.1 and 0.3 mm spatial resolution [10,16]. Moreover, roughness is automatically reduced through the EEM process in the high spatial frequency range. Finally, a maximum of an 1 m long X-ray mirror with the peak to valley (PV) of 1 nm was fabricated [17]. However, since the chemical reaction proceeded at the atomic scale, the removal rate is only 1×10^{-4} $mm^3 \cdot h^{-1}$.

Achieving atomic-scale machining fundamentally requires the discovery or application of phenomena distinct from conventional macroscopic processes. Chemical mechanical polishing (CMP) is widely employed for obtaining ultrasmooth surfaces [18]. During CMP, the chemical slurry first modifies the substrate surface, and then mechanical abrasives remove the soft modified layer [19]. However, corrosive and toxic components are normally used in conventional CMP [20]. To overcome this pollution, the environmentally friendly CMP has been developed [21,22]. Furthermore, a cross-scale model was constructed for CMP, elucidating the fundamental mechanism of CMP and atomic-scale polishing [23].

Hydroxyl (OH) groups play an important role in chemical bonding between surfaces. Previously, an abrasive-free finishing technology known as catalyst-referred etching (CARE) was developed [24]. Hara et al. [25] reported that silicon carbide (SiC) can be etched in hydrofluoric acid (HF) solution by using a platinum (Pt) catalyst as a tool. Isohashi et al. [26] demonstrated that using only a Pt catalyst in pure water can smooth the SiC surface directly. A Sq roughness of 0.05 nm can be achieved. Bui et al. [27,28] revealed the mechanism of CARE using density functional theory. First, a F^- ion adsorbs to the Si step edges, forming a five-coordinate structure in a metastable state (MS). The Pt–O–Si bond formed and reduced the total energy of MS. Then, a proton was transferred to rupture the Si-C back bonding. In pure water, the role of OH^- is the same as that of F^- in CARE. Thus, the catalyst is utilized to promote the generation of F^-/OH^- and form Pt–O–Si bonds to stabilize the hypervalent silicate state. However, post-processing byproducts covered the catalyst surface, leading to a severe reduction in the removal rate. Toh et al. [29] proposed *in situ* cyclic dissolution and electroplating of the catalyst to stabilize a high removal rate. Furthermore, Toh et al. [30] studied how to reduce the adsorption energy of byproducts, and a Ru-based alloy catalyst was developed to recover catalyst activity. Accordingly, the generation of OH and Pt–O–Si bond formation are important for chemical-based material removal.

In addition to inorganic and metal polishing pads, organic polymer materials are gaining attention because of their hydrolytic properties. For instance, the ester bond can be hydrolyzed into a carboxyl group (COOH) in pure water, which is well known in the field of organic chemistry [31,32]. On the basis of the hydrolysis reaction of polymethyl methacrylate (PMMA), water polishing using a PMMA plate was proposed by Guo et al. [33]. Atomic-level smoothing of glass (0.073 nm Sq roughness) and silicon (0.037 nm Sq roughness) surfaces was achieved. This hydrolysis reaction generates active groups on acrylic, and C–O–Si bridge bonds are formed at the interface [34]. Egawa et al. [35] and Matsuzawa et al. [36] developed organic abrasive machining (OAM) for high spatial resolution figuring [35,36]. By utilizing an elastic tool with acrylic particles slurry, OAM was used to obtain a 100 μm machined spot. However, the removal rate is limited by the low hydrolysis reaction rate in pure water, which is only 9 $nm \cdot h^{-1}$ for SiO_2 [33].

The direct application of organic polymers as polishing tools, as demonstrated by Guo et al. [33], reveals significant potential for advancing machining technologies through novel organic material strategies. Persistent polymer accumulation poses significant environmental challenges. Consequently, biodegradable polymers have garnered significant interest for mitigating plastic pollution. Among them, polybutylene succinate (PBS), polylactic acid (PLA), and polycaprolactone (PCL) are widely used [37]. Enzymatic hydrolysis is considered one of the most effective degradation methods for these polyesters [38,39]. Rosato et al. [40] studied the ability of several hydrolytic enzymes—namely, esterases, lipases, proteases, and cutinases—to promote the

hydrolysis reaction rate of polyesters. It was demonstrated that only cutinase can fully degrade PBS, whereas PLA cannot be completely degraded by any enzymes. Zumstein et al. [41] reported that hydrolyzability increased with increasing flexibility of the polyester chain segments and the access efficiency of enzyme active sites. Di Bisceglie et al. [42] studied the feasibility of polyurethane hydrolysis using *Humicola insolens cutinase* (HiC). Almeida et al. [43] studied the hydrolysis of PCL by an esterase from the archaeon *Archaeoglobus fulgidus* using molecular dynamics simulation. The overall energy barrier of enzymatic hydrolysis was 12.9 kcal·mol^{-1}, indicating that the chemical step is very efficient. In this context, enzymes are very effective at increasing the hydrolysis rate of a polymer.

In 1993, biomachining was proposed by Yoshiyuki et al. [44] for metal removal. Biomachining uses microorganisms such as *Acidithiobacillus ferrooxidans* to remove metal material [45]. Material removal is an indirect process. First, microorganisms oxidize ferrous ions (Fe^{2+}) into ferric ions (Fe^{3+}). The Fe^{3+} subsequently oxides the metal, causing it to dissolve [46,47]. Enzymatic biomachining was proposed by Eskandarian et al. [48] to remove copper using glucose oxidase. Glucose oxidase catalyzed the glucose oxidation reaction to produce hydrogen peroxide (H_2O_2). Afterward, H_2O_2 oxidized Fe^{2+} to Fe^{3+}, and material removal was achieved. In fact, microorganisms or enzymes directly or indirectly oxidize Fe^{2+} and do not participate in the metal removal process. Moreover, this method is limited to some metals that can only be oxidized and dissolved; thus, it cannot be applied to semiconductors and optical materials. The *A. ferrooxidans* bacterium used in the process can grow and act only in an acidic (pH = 1–3) environment [49]. However, the achievement of atomic-scale polishing or figuring by biomachining has not yet been reported.

Inspired by biological enzymatic degradation studies, we propose an enzymatic hydrolysis machining (EHM) technique in this study. The core of EHM is that the enzymes promote the hydrolysis reaction of the polymer, continuously generating a large number of new reactive groups. Focusing on the challenges of machining X-ray mirrors, we aimed to develop EHM for atomic-scale polishing and figuring that achieves crystallographic perfection. An experimental setup was developed for the EHM process. Static incubation experiments were carried out to confirm the enzymatic hydrolysis phenomenon through morphology observation and chemical analysis. The material removal capabilities of Si under aqueous and enzymatic conditions were verified and compared. The machining footprints of pad-type and wheel-type polymer tools were investigated for polishing and figuring. The polishing characteristics of EHM are presented. Furthermore, EHM was extended to other materials, and numerically controlled EHM was deployed specifically for large-scale Si mirrors.

2. Experimental methodology

2.1. Polymers and enzymes

As typical biodegradable materials, PBS and PCL were used to verify the enzymatic hydrolysis process and material removal capability. A damping cloth pad is a typical industry standard soft polishing pad that is used in the final finishing process during CMP. The damping cloth is composed of PU, which can be hydrolyzed by enzymes. Here, it was used as a polishing pad in EHM. All the polymer materials were commercially available. Lipase from *Rhizopus oryzae* (RoL), lipase B from *Candida antarctica* (CALB), and cutinase from HiC were selected for the experiments. We selected these three enzymes for two reasons. First, we investigated whether these enzymes can effectively degrade PBS and PCL through literature research [40–42]. Second, they are widely used in biological research and are commercially available. CALB and HiC were purchased from Novozymes (Danmark), while RoL was purchased from Sigma-Aldrich (USA). These enzymes were stored in a refrigerator at 0–10 °C.

2.2 Experimental setup

A static incubation experiment was carried out to assess the morphological changes in the polymer pads after immersion in the enzyme. As shown in Fig. 1(a), PBS and PCL plates were incubated separately in RoL, CALB, and HiC solutions in a closed desiccator. The hydrolysis rate can be elevated by raising the temperature, which enhances the activity of biological enzymes. For most enzymes, this process is optimal at approximately 40 °C. To make the enzymatic hydrolysis phenomenon more observable, the incubation temperature was set to 40 °C. All parameters remained consistent: enzyme solution volume (10 mL), temperature (40 °C), and incubation duration (24 h). Specific experimental details are provided in Table 1. The polymer pads were 15 mm in diameter and 2 mm thick.

Table 1

Static incubation experimental parameters.

Journal Pre-proofs

No.	Polymer	Enzyme
1	PBS	RoL
2	PCL	RoL
3	PBS	CALB
4	PCL	CALB
5	PBS	HiC
6	PCL	HiC

Single-crystal silicon (Si) substrates with an orientation of (100) were commercially available. The size of the workpiece was 40 mm × 40 mm × 10 mm, as presented in Fig. 1(b). The substrates used in experiments were preprocessed by CMP. An experimental setup was developed for the proposed EHM process, and its configuration is shown in Fig. 1(c). It was composed mainly of a loading system, rotation motor, 3-axis motion stage, polishing pad, and enzyme solution. The experimental loading force was applied by adding standard weights and calibrated by the force sensor before each experiment. The Si substrate and polymer polishing pad were immersed in an enzyme-filled sink. Thus, experiments can be performed under loading force and axial motion. A photo of the experiment in the HiC enzyme solution is presented in Fig. 1(d). The inset photo was the used damping cloth polymer pad. The diameter of the pad was 15 mm. Accordingly, EHM has several advantages, such as being slurry/abrasive-free, simple and cost-effective, and environmentally friendly without the use of acid or alkaline solutions. EHM is conducted in an atmospheric environment at room temperature without thermal effects, making it an effective approach for the practical machining of large and even complex curved workpieces. Like subaperture machining methods based on polishing pads and slurries, EHM is compatible with current commercial processes and equipment. The critical experimental parameters are recorded in Table 2.



(a)

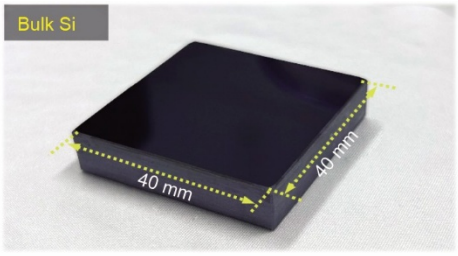

(b)

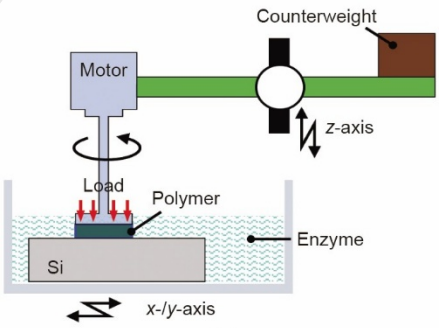

(c)

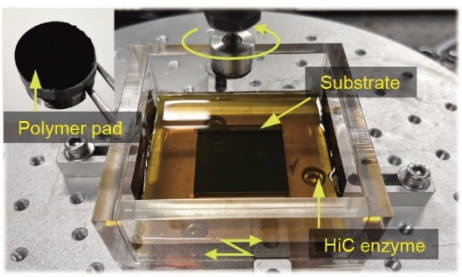

(d)

Journal Pre-proofs

Fig. 1. (a) Photograph of the static incubation experiment. PBS and PCL were incubated in RoL, CALB, and HiC solutions. (b) Photograph of the Si substrate. (c, d) Experimental setup of EHM: (c) schematic diagram and (d) photograph.

Table 2

Experimental conditions.

Parameters	Values
Substrate	Si: 40×40×10 mm^3 (CMP preprocessed)
Loading force	2–15 N
Rotation speed	50–1000 $r \cdot min^{-1}$
Working duration	0–12 h
Enzymes	RoL, CALB, and HiC

2.3. Characterizations

All the polymer plates and substrates were subjected to ultrasonic cleaning with deionized water and ethanol for 5 min. Subsequently, we dried the substrates using nitrogen gas. The morphologies of the polymer pads were obtained utilizing a scanning electron microscope (SEM; Zeiss Merlin, Germany). A platinum layer with the thickness of 10 nm was sputter-deposited to the polymer surfaces to ensure adequate electrical conductivity. Attenuated total reflection Fourier transform infrared spectroscopy (ATR-FTIR; Bruker Vertex 70v, Bruker, Germany) was employed to analyze the chemical composition of the polymers, with each spectrum recorded over the wavenumber range of 4000–500 cm^{-1} using 64 scans with a spectral resolution of 2 cm^{-1}. The Si removal traces induced by the PBS and PCL tools were quantified utilizing scanning white light interferometry (SWLI; Zygo NewView™ 9000, Zygo, USA) in stitching mode. For substrates polished with a damping cloth, the removal profile and volume were determined through a laser interferometer (Tyggo INF150V-LP, Tyggo, China). Specifically, we tested the surface height error data both before and after processing, and the two datasets were subtracted to derive the removal pattern. The chemical states of the PBS tool surfaces before and after EHM were investigated via X-ray photoelectron spectroscopy (XPS; Quantum 2000, ULVAC-PHI, Japan). Surface roughness was characterized through an atomic force microscope (AFM; Bruker Dimension Edge, Bruker). Cross-sectional observations of the Si subsurface were investigated through a transmission electron microscope (TEM; FEI Titan Themis 2000, FEI, USA), with sample preparation accomplished via a focused ion beam equipment (FIB; Helios 450S, FEI).

2.4. Proposed EHM

Enzymes are protein-based biological catalysts that accelerate chemical reactions. Hydrolases, a subclass of enzymes, specifically catalyze the hydrolysis of chemical bonds—a reaction in which water molecules cleave bonds. With respect to ester bonds (–COO–), the hydrolysis reaction produces carboxylic acid (–COOH) and alcohol (R-OH) moieties. OH groups have strong oxidizing properties and are widely used in the field of manufacturing. However, polymer hydrolysis rates in pure water remain weak, limiting the application of polymers in the machining process. Enzymatic catalysis significantly enhances hydrolysis kinetics, enabling the continuous regeneration of active OH groups.

The enzymatic hydrolysis mechanism involving enzymes and polymer substrates is shown in Fig. 2. Unlike conventional petroleum-derived polymers, biodegradable polymers demonstrate enhanced hydrolytic susceptibility. Using PBS as a representative biodegradable polyester, Fig. 2 depicts its hydrolysis pathway: enzymatic catalysis cleaves polymer chains into monomers that subsequently degrade them into succinic acid and 1,4-butanediol. This reaction exposes abundant terminal COOH and OH functional groups on the PBS surface. This fundamental process involves enzymatic hydrolysis, wherein biological catalysts first initiate polymer chain scission. The resulting hydrolyzed monomers then diffuse into the surrounding solution, while fresh COOH and OH functional groups are continuously regenerated on the polymer surface through ongoing chain cleavage.

The schematic in Fig. 2 depicts the atomic-scale removal mechanism for EHM. First, when the workpiece is immersed in pure water, hydroxyl groups (OH) adsorb onto its surface. Concurrently, enzymatic hydrolysis generates abundant COOH and OH reactive groups on the polymer surface. Second, the polymer and substrate are in contact, and a dehydration reaction occurs at the interface under a loading force. As depicted in Fig. 2, the carboxyl groups (COOH) derived from the polymer react with the OH present on the substrate to generate C–O–Si bridging bonds. These bridge bonds may weaken the binding force between surface Si atoms and subsurface layers. Afterward, under the shearing effect, the Si–Si bond between the surface and subsurface atoms breaks, and the Si atoms are removed. However, the accumulation of reaction byproducts (C–O–Si complexes) on the polymer surface eventually inhibits further reactions. Enzymatic hydrolysis continuously cleaves polymer chains, releasing these byproducts along with monomers into solution. The polymer surface is refreshed by this enzymatic hydrolysis process, and abundant OH groups are produced again. The above reactions occur continuously and repeatedly, allowing for the EHM to effectively remove materials. Thus, the roles of the enzymes can be elucidated from two aspects. First, enzymes catalyze the hydrolysis reaction and generate a large number of OH groups. Afterward, enzymatic hydrolysis removes the postproducts covering on the polymer surface and continuously refreshes it.

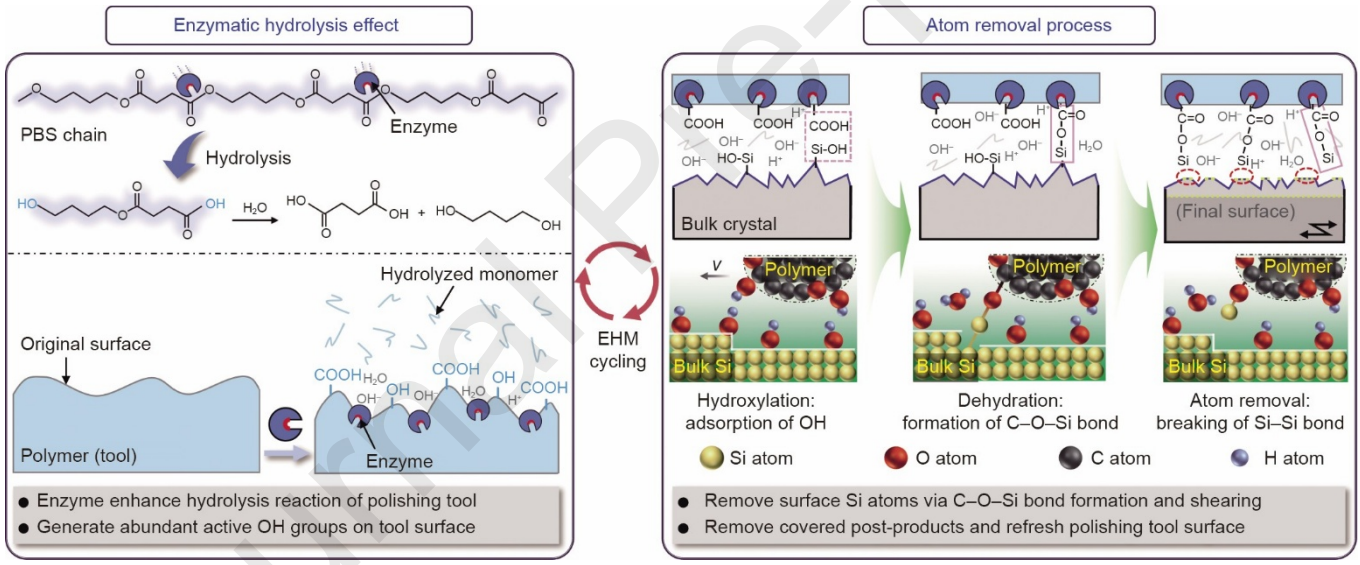

Fig. 2. Schematic illustration of the enzymatic hydrolysis effect and material removal mechanism of EHM.

3. Results and discussion

3.1. Enzymatic hydrolysis of polymers

EHM employs a biological phenomenon wherein enzymes catalyze the hydrolysis of polymeric chains. Consequently, experimental validation is essential for confirming this enzymatic hydrolysis phenomenon. Although PBS and PCL are inherently biodegradable, their degradation in pure water typically requires several weeks to manifest visibly. In the practical EHM process, however, the polymer tool undergoes pressurized rotational motion, and interfacial friction dynamically affects its morphology. Thus, directly observing the effects of enzymatic hydrolysis is difficult.

Therefore, a static incubation experiment was performed. The incubation conditions are shown in Table 1. As depicted in Fig. 3, the PBS and PCL surfaces clearly exhibited signs of hydrolysis following incubation in the three enzyme solutions. Initial polymer plates were uniformly lapped with 3000-grit sandpaper prior to testing, creating directionally aligned scratches visible in the as-received PBS and PCL SEM images. The insets show schematic molecular structures of each polymer. After 24 h of

immersion in pure water, the morphologies of the PBS and PCL did not change, and there was no sign of hydrolysis. The hydrolysis of the polymers in pure water was very weak. After 24 hours of incubation in RoL and CALB solutions, pitting clearly emerged across the PBS surface, with cavities penetrating deeply into the material. This erosion morphology demonstrated efficient enzymatic adsorption and hydrolysis. PBS degradation was particularly pronounced in the HiC solution, where the surface developed fibrous textures and the original abrasion marks completely disappeared. For the PCL plates, distinct cracking was observed following incubation in the RoL and CALB solutions. CALB exposure caused particularly severe enzymatic erosion, resulting in substantially damaged and roughened surfaces. In contrast, the HiC enzyme induced relatively mild surface degradation of PCL. These results validate the efficacy of all three enzyme solutions in hydrolyzing PBS and PCL substrates.

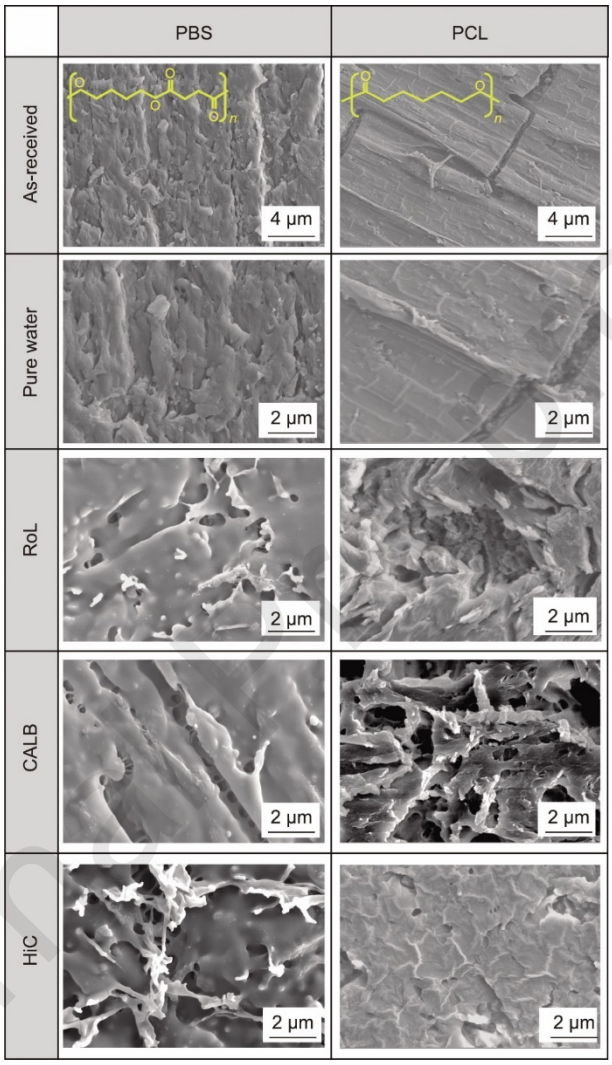

Fig. 3. Enzymatic hydrolysis phenomenon. Morphologies of the polymer pads before (as received) and after (pure water) incubation in pure water, RoL, CALB, and HiC enzyme solutions.

In addition to morphological analysis, molecular-level characterization of post hydrolyzed polymer surfaces is essential. ATR-FTIR spectroscopy was employed to examine surface chemical modifications before and after aqueous/enzymatic incubation. This technique combines infrared spectroscopy with ATR sampling to probe material composition in a vacuum condition. Three PCL plates (as-received, water-incubated, and HiC-incubated) were put in a closed desiccator at 50 ℃. After immersion for 24 h, these plates were cleaned with water and subsequently dried with nitrogen gas. Thus, the hydrolysis products and adsorbed enzymes on the polymer surface were removed cleanly. Then, the plates were dried in the desiccator at 50 ℃ for 12 h to remove water.

As presented in Fig. 4, the ATR-FTIR spectra of the three PCL specimens reveal distinct molecular features. Characteristic absorption bands were evident at 2920 and 2850 cm^{-1}, attributing to the symmetric and asymmetric CH_2 stretching vibrations of PCL, respectively [50]. The prominent peak at 1720 cm^{-1} was corresponded to the C=O stretching vibration, confirming the

presence of ester linkages [51]. Additionally, the band observed at 1240 cm^{-1} arises from C–O–C stretching vibrations associated with the ester functional groups [52]. Critically, comparative spectral analysis indicates that neither aqueous nor enzymatic incubation significantly altered the fundamental molecular architecture of PCL. However, quantitative examination demonstrates a progressive decrease in the intensity of the carbonyl (C=O) stretching band: decreasing from 1.69 (as-received) to 1.34 following water immersion, and further diminishing to 1.05 after HiC enzyme treatment. These significant attenuation phenomena provide direct spectroscopic evidence of hydrolysis occurring in both aqueous and enzymatic environments, indicative of ester bond cleavage and subsequent monomer release. Notably, the more pronounced intensity reduction observed under enzymatic conditions reflects an accelerated hydrolysis rate compared to purely aqueous hydrolysis. Consequently, the enzymatic hydrolysis effect was demonstrated clearly from intuitive morphological observation and spectroscopic analyses.

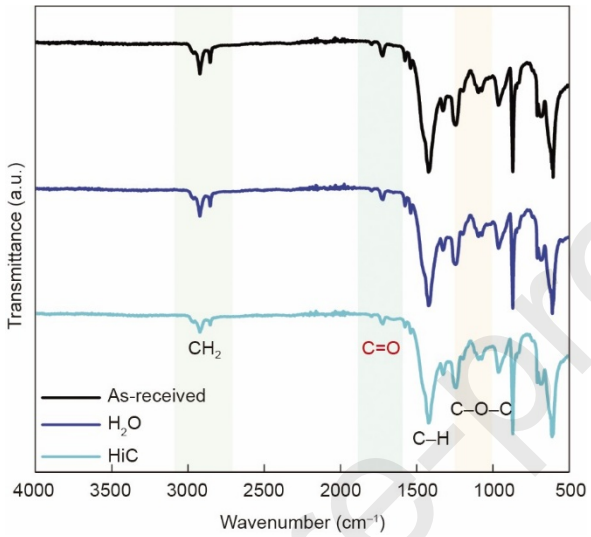

Fig. 4. ATR-FTIR spectra analysis of surface chemical composition of PCL plates: as-received, water-incubated, and HiC-incubated.

3.2. Material removal of Si

Enzymatic hydrolysis generates abundant reactive sites on polymer surfaces. By utilizing this enzymatic hydrolysis effect, confirming the ability of polymer tools to remove Si atoms from the enzyme solution is indispensable. The important role of enzymatic hydrolysis in removing materials can be revealed through comparison with that of processing in pure water. This comparison is essential for demonstrating that compared with pure water, EHM can achieve the atomic-scale removal and that enzymes could promote the material removal rate (MRR) of Si.

A schematic diagram of the setup for removal experiments is displayed in Fig. 5(a). A ball-type polymer tool was employed. To avoid having no rotation speed in the center, the polymer tool was tilted at a certain precession angle. The sample was then reciprocated under a loading force. Both the polymer tool and the substrate were placed in pure water or an enzyme solution. The experimental loading force was 5 N. The rotation speed was 1000 $r \cdot min^{-1}$. The reciprocating step was 8 mm, and the processing time was 12 h. The precession angle was 3°. The used PBS polymer tool has a diameter of 15 mm, which was imaged in Fig. 5(b). Processed traces were measured via SWLI, stitched with a viewing area of 1.56 mm × 1.56 mm. The removal trace is clearly depicted in Fig. 5(c). The Si removal depth was determined as 16.4 nm under pure water conditions. This means that the MRR was approximately only 1.37 $nm \cdot h^{-1}$. Although the removal rate was very low, it showed that PBS had the ability to remove Si atoms in pure water without abrasives. Moreover, the material removal depth can be precisely regulated at the atomic scale. However, the removal depth and width are very unstable, limiting the use of polymers as machining tools. As depicted in Fig. 5(d), the removal depth of Si via PBS in the HiC enzyme significantly increased. As shown in the removal profile in Fig. 5(e), the removal depth was 213.5 nm. The removal rate was 17.8 $nm \cdot h^{-1}$ (13 times higher than that in pure water). The EHM-processed grooves were stable, and the width and depth were uniform. Furthermore, the removal stability under long working durations using HiC is presented in Fig. S1 in Appendix A.

To investigate the underlying removal mechanism, we analyzed the surface chemical state of the PBS tool before and after EHM processing using XPS. The survey scan in Fig. 5(f) clearly reveals Si2s and Si2p signals after processing. The details of the atomic concentration are displayed in Table 3. The atomic concentration of Si increased from 0.8 to 2.6 after processing. This demonstrated that chemical etching occurred between the PBS and Si interface. Generally, glass fibers are added during the

production process of PBS plates to enhance their mechanical properties. This explains why the surface of the as-received PBS tool contains Si. The region scans of C1s before and after processing are shown in Fig. 5(g). The C1s spectra can be attributed to three peaks according to binding energy: –COO– (288.6 eV), –C–O– (286.3 eV), and –C–C– (284.8 eV) [53]. The –COO– peak was attributed to the ester bonds in PBS and the carboxyl groups of the hydrolysis products. After EHM processing, a peak attributed to carbonyl C=O at 287.7 eV appeared [53,54]. This revealed the hydrolysis reaction of PBS in the HiC enzyme. Moreover, the C1s concentration decreased from 78.1% to 70.7%, whereas the O1s concentration increased from 17.3% to 23.5%. As the hydrolysis reaction progresses, the decrease of the C content can be attribute to dissolution of the hydrolyzed monomers into the water or enzyme solution. As shown in Fig. 5(h), the Si–O–C peak (102.7 eV) implied chemical bonding between Si and the polymer tool [55]. It is a dehydration reaction process, and its intensity obviously increases after processing. Thus, the Si atoms are removed through the chemical bonding through Si–O–C bridge bond.

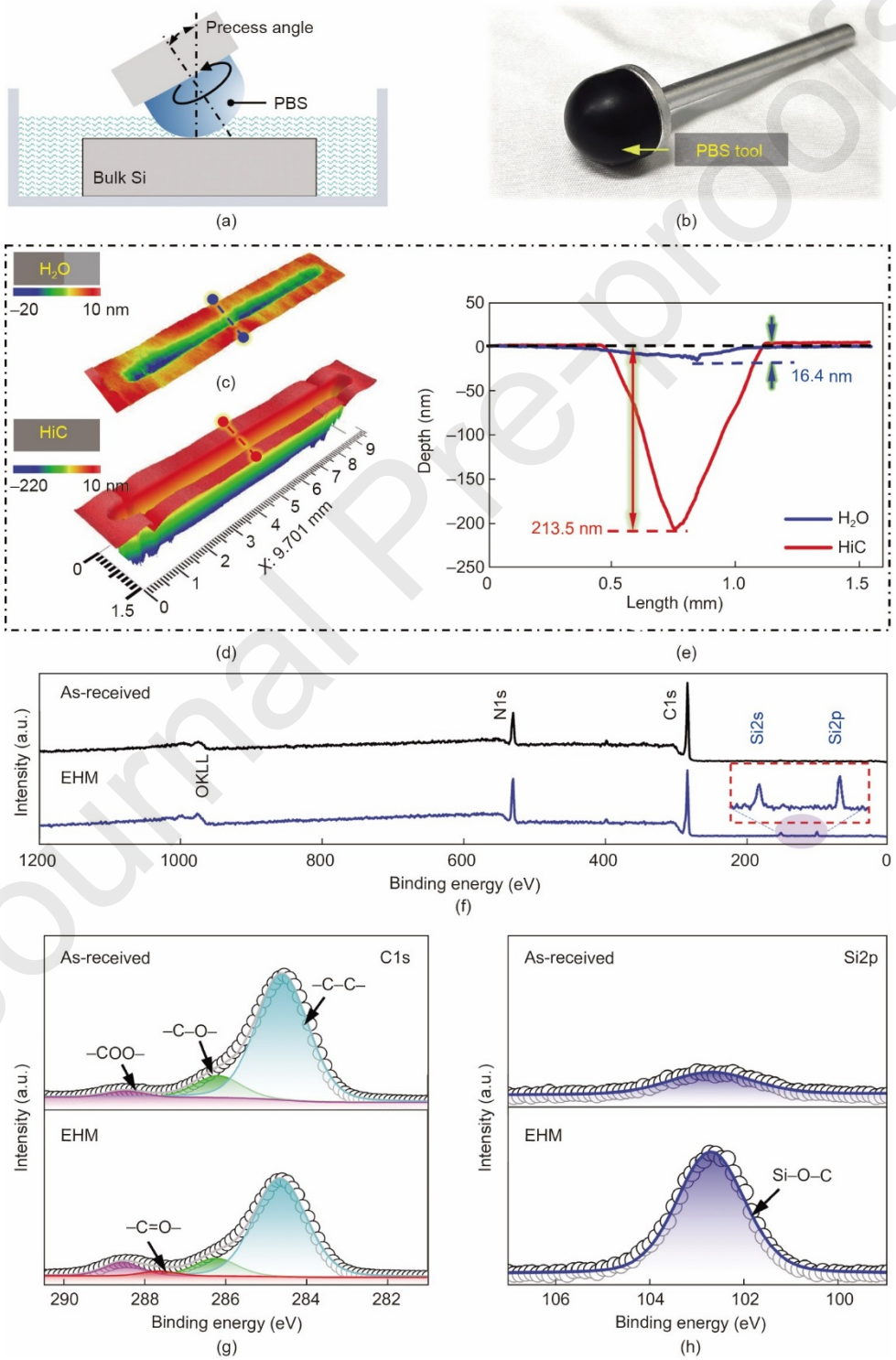

Journal Pre-proofs

Fig. 5. Material removal capability of Si via EHM and XPS analysis of PBS tool. (a) Schematic of the setup for the material removal experiment. (b) Photograph of the ball-type PBS tool. (c, d) Removal topographies of Si in (c) pure water and (d) HiC enzyme solution. (e) Removal profiles of Si in pure water and HiC enzyme solution using PBS tool. (f) The survey scan of as-received and EHM-processed PBS. (g, h) The region scans of C1s and Si2p.

Table 3.

Atomic concentration of the PBS surface before and after EHM.

Atomic (%)	As-received	EHM-processed
C1s	78.1	70.7
O1s	17.3	23.5
Si2p	0.8	2.8

As these reactions occur at the atomic scale, EHM is an atomic-scale manufacturing technology. Notably, any polymers containing hydrolysable groups, such as polyesters (PLA, PCL, and PBS, etc.), polyamides (PA6, etc.), and polyurethanes (PU, etc.), can work as a tool material with the catalysis of specific enzymes for material removal. Thus, EHM offers broad applicability for enzymes, polymer tools, and workpieces. In addition, EHM removes materials purely through chemical reactions, and the polymer is much softer than the substrate. Thus, surface and subsurface damage would not be introduced by EHM.

3.3. Process optimization

Fig. 6(a) shows the trench removal pattern under 5 N and a rotation speed of 300 r·min^{-1}. The precession angle was 3°. Six trenches were formed after 6 h of processing to evaluate the removal stability. The removal profile was displayed in Fig. 6(b). We took the average removal depth of the six grooves as the final value, and the standard deviation as an error bar to present the removal stability. As shown in Fig. 6(c), HiC and CALB were effective for the removal of Si via the PBS and PCL tool. For the HiC enzyme, the removal depth of Si can reach 54.2 and 82.3 nm using PBS and PCL, respectively. Meanwhile, the removal depths of Si were 71.5 and 60.7 nm for PBS and PCL when using the CALB enzyme. For RoL enzyme, the removal depth of Si was only 16.2 nm for the PBS tool, suggesting RoL promotes the hydrolysis reaction of PBS very slightly. In contrast, RoL was effective for PCL, and the removal depth reached 114.8 nm. Fig. 6(d) shows the relationship between rotation speed and removal depth. Other parameters were constant as shown in Fig. 6(c), and the rotation speed was increased from 100 to 900 r·min^{-1}. The removal depth was increased with rotation velocity nearly linear from 6.0 to 30.0 nm. Based on the Preston equation, the removal rate increases with rising rotational speed and loading force. Therefore, a higher rotation speed was preferred to achieve a higher removal rate for EHM. Fig. 6(e) shows the relationship between work duration and removal depth. The removal depth increased with increasing work duration from 2 to 12 h. Fig. 6(f) depicts the relationship between loading force and removal depth. The removal depth was found to increase with rising loading force. However, the removal depth exhibited a faster increase as the loading force went up from 3 to 7 N. When the loading force increased further from 7 to 13 N, the removal depth increased slowly and approached saturation. This effect likely arises from polymer tool wear, which expands the interfacial contact area and consequently affects material removal depth.

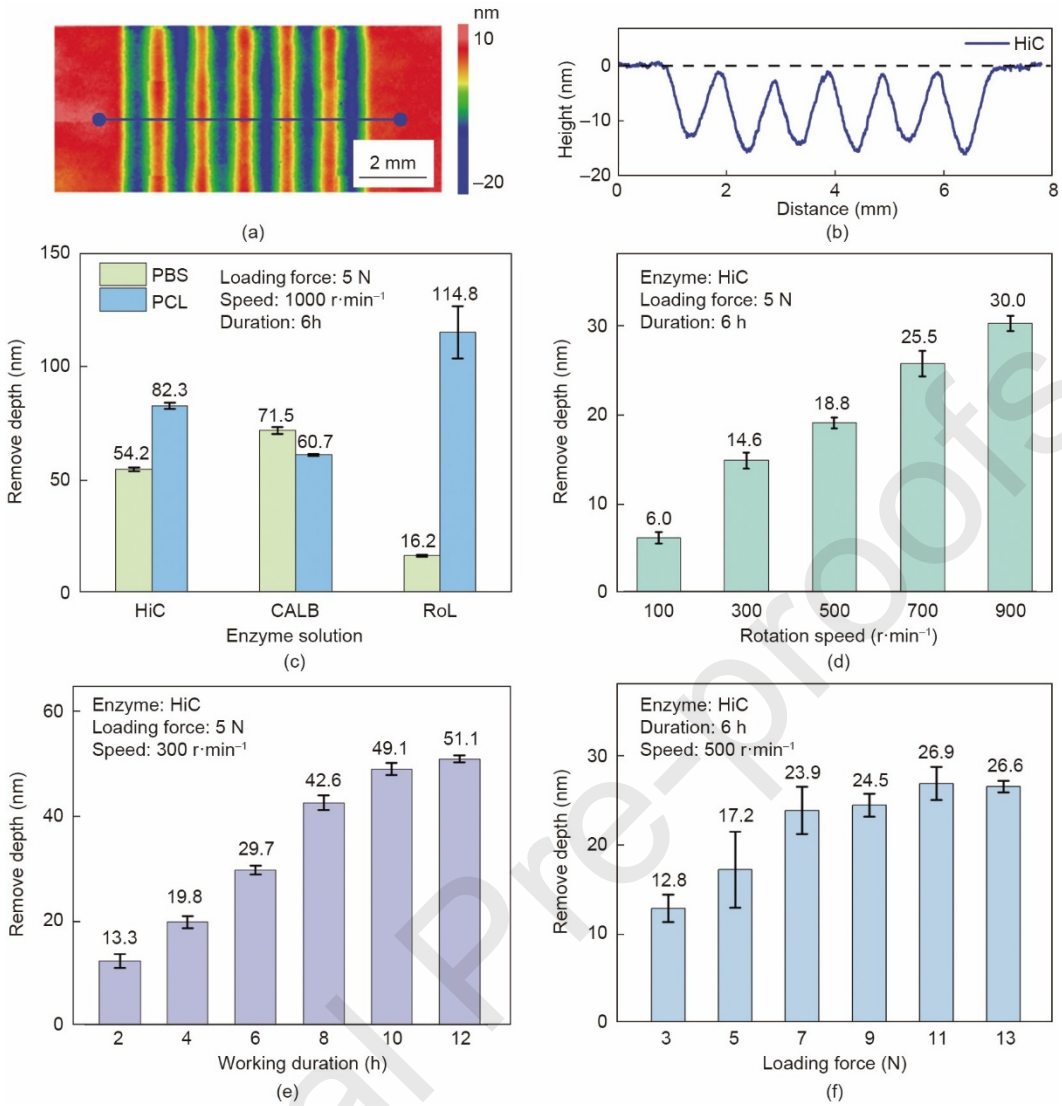

Fig. 6. Parameter optimization of the EHM process. (a) Trench removal pattern and (b) profile of removal depth. Effect of (c) enzyme solution, (d) rotation speed, (e) working duration, and (f) loading force on removal depth. Each error bar corresponds to the standard deviations obtained from depth measurements of six trenches.

3.4. Machining footprints for polishing and figuring

Since material removal can be achieved via the enzymatic hydrolysis effect, different removal patterns can be constructed. A pad-type tool was used for polishing, whereas a wheel-type tool was used for figuring. Polishing works at the microscale at mid-to-high spatial frequencies. It achieves relatively uniform material removal without targeting localized areas, thereby reducing surface roughness under reference shearing action. In contrast, figuring works at the macro scale and has a low spatial frequency. It enables localized and controllable material removal in specific regions. Through precise control of the dwell time, localized material removal is accurately managed to achieve form error correction on the whole surface. Actually, we used PBS/PCL for the experiments directly. However, it was difficult for the PBS and PCL plate to contact the Si substrate well because of its high hardness. Scratches were easily generated during the experiments. Therefore, a commercially soft polymer material (damping cloth pad) was used for the experiments. The damping cloth pad had a shore-A hardness of 54. Static dwell processing of EHM was performed to obtain the machining footprints in the HiC enzyme solution.

The results for the pad-type polymer tool are depicted in Fig. 7(a). The pad has a diameter of 15 mm. The damping cloth pad rotated on the Si surface for 3 h without axis motion, with a loading force of 5 N and a rotation speed of 100 r·min^{-1}. As shown in Fig. 7(b), a removal footprint can be clearly observed. The removal depth was only 53.1 nm. The volume removal rate (VRR) was 3.79×10^{-5} mm^{3}·min^{-1}. Since the removal rate was proportional to the rotation velocity, the removal function was W-shaped.

These results were consistent with those of conventional abrasive-based machining methods. Under the reference effect of the polishing pad, the surface asperities preferentially contact the pad and are removed.

As a precision machining method, EHM should achieve controlled material removal to form the desired surface. By using a wheel-type polymer tool, EHM can be used for surface mapping, as shown in Fig. 7(c). The wheel was made of polyurethane rubber with a diameter of 80 mm. Different kinds of polyurethane rubber can be used as wheel-type tools. The rubber used here had a shore-A hardness of 90. Its tolerance of a spherical shape was controlled by single-point diamond turning, and the wheel surface was turned into a spherical surface 80 mm in diameter and 10 mm thick. The damping cloth pad was attached to the polishing wheel. The damping cloth wheel was rotated under a loading force and immersed in HiC enzyme solution. The loading force was 3 N. The rotation speed was 80 $r \cdot min^{-1}$, and the working duration was 30 min. As depicted in Fig. 7(c), a Gaussian-like removal function was formed. From the horizontal profile, it has a removal depth of 56.7 nm and a full width at half maximum of approximately 4 mm. The VRR was 3.87×10^{-5} $mm^3 \cdot min^{-1}$, demonstrating that EHM has atomic-scale removal capabilities.

In contrast, a 1 $nm \cdot min^{-1}$ removal rate can be achieved in EEM, while a VRR of 14×10^{-14} $m^3 \cdot h^{-1}$ (2.3×10^{-6} $mm^3 \cdot min^{-1}$) was reported for evaluating stability [10]. When Pt was used as a catalyst in pure water in CARE, the MRR for the 4H-SiC wafers with a 4°-off-axis was 19 $nm \cdot h^{-1}$ [26]. The MRRs reached 6.6 $nm \cdot h^{-1}$ when it was applied to crystalline quartz and 200 $nm \cdot h^{-1}$ when it was applied to silica glass [56]. In OAM using acrylic abrasives, the removal rate was 604 $\mu m^3 \cdot min^{-1}$ (6.04×10^{-7} $mm^3 \cdot min^{-1}$) for fused silica [36]. Notably, removal rates were influenced by tool/workpiece dimensions and process parameters. Overall, EHM exhibited a material removal capability on the order of $nm \cdot h^{-1}$, which was comparable to that of other existing polishing or figuring technologies.

We measured the surface roughness in the machining footprints. The approximate locations of the measurements are marked in Fig. 7(b) and (c). In a 1μm × 1 μm viewing area, the initial surface roughness was recorded as 0.21 nm Sq. The scratches can be clearly seen in Fig. 7(d). The Sq roughness was 0.086 nm in the pad-type removal footprint, demonstrating that atomic-level smoothing can be achieved. Notably, the roughness was 0.059 nm in the footprint of the wheel-type tool. These results show that when EHM was used for figuring, the microroughness could be reduced to the atomic level simultaneously.

Journal Pre-proofs

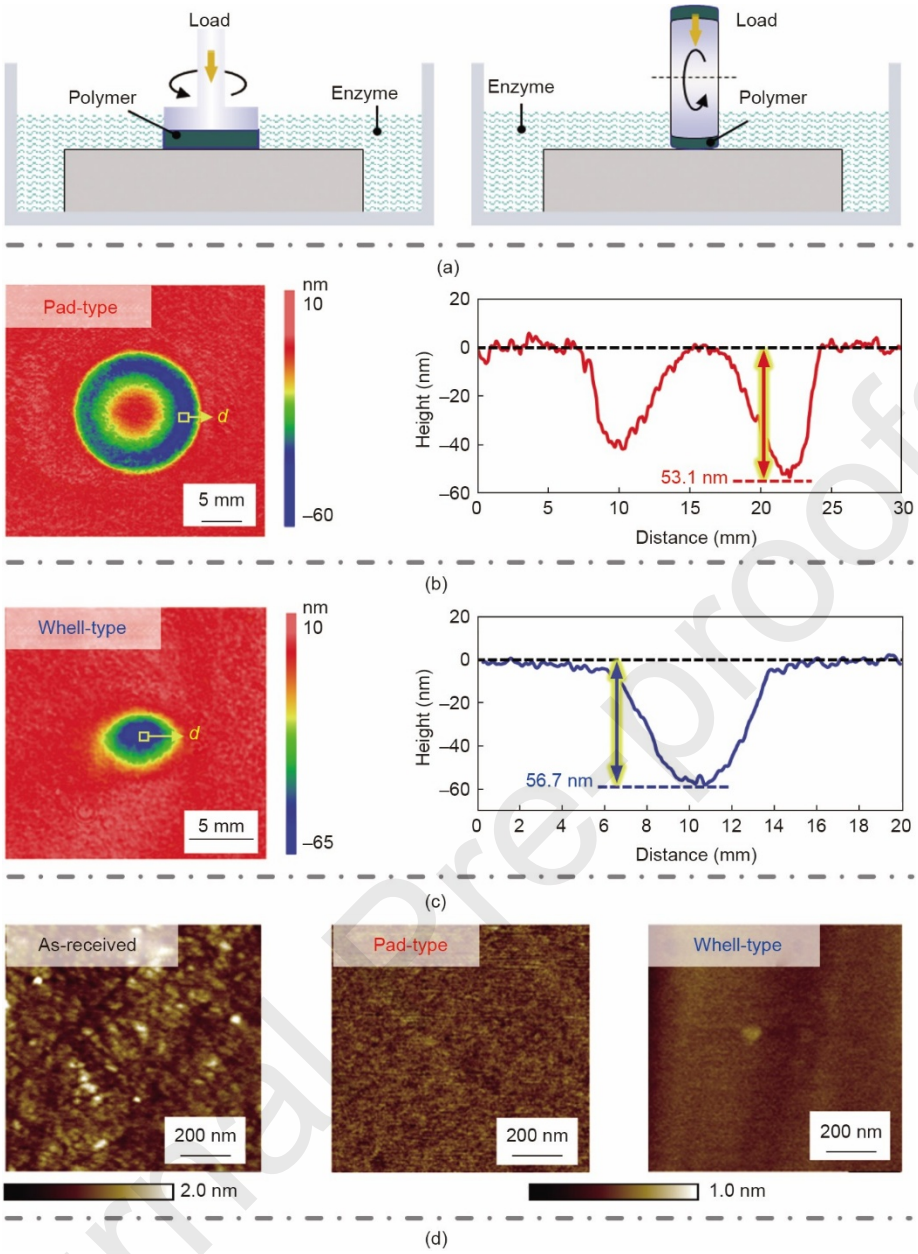

Fig. 7. Machining footprints via EHM. (a) Schematic of the pad-type and wheel-type polymer tools for polishing and figuring. (b, c) Removal patterns and profiles of Si via (b) pad-type and (c) wheel-type polymer tools. (d) AFM topographies and roughness of Si as-received (Sq: 0.21 nm) and after single-point dwell processing via Pad-type (Sq: 0.086 nm) and Wheel-type (Sq: 0.059 nm) tools.

3.5. Polishing characteristics of EHM

3.5.1. Atomic-level smoothing of Si

The damping cloth was a commercial soft polishing pad made of polyurethane, which was generally used as the final fine finishing process in CMP. The pad mainly carries the polishing slurry and contacts the substrate surface. However, the polishing pad alone cannot remove material without the use of slurry or abrasives. A photograph of the used damping cloth polishing pad is shown in Fig. S2(a) in Appendix A. The diameter is 15 mm. The morphology clearly observed by SEM is shown in Fig. S2(b) in Appendix A. The vertically oriented pore structures with a compressible substrate were conducive to the storage of water or enzyme solution. The inset shows the molecular structure of the urethane (–NHCOO–) bond.

Under the conditions of 5 N and 100 r·min^{-1}, a line reciprocating path of 20 mm was processed for 12 h to observe the material removal. As demonstrated in Fig. 8(a), only the damping cloth pad in pure water did not result in material removal for Si. In

contrast, in the HiC enzyme solution, the removal morphology was significant and uniform, as displayed in Fig. 8(b). As shown in the profiles in Fig. 8(c), the removal depth in the HiC enzyme solution was 63.8 nm, whereas no material was removed in pure water. These findings show that the HiC enzyme can directly hydrolyze commercial CMP polishing pads and that material removal can be achieved without the use of a chemical slurry or mechanical abrasives. This finding verifies the effectiveness of the EHM.

The relationship between the roughness variation over time for processing in the enzyme and pure water is demonstrated in Fig. 8(d). We measured the roughness in a viewing area of 1 μm × 1 μm every hour, and the total processing duration was 4 h. The roughness value in the figure was obtained by taking the average value of the six randomly measured data points. In pure water, the roughness decreased very slowly. The roughness changed little after one hour of processing, from 0.26 to 0.25 nm. After 4 h of polishing, it decreased to 0.20 nm, which indicated that the smoothing efficiency was very limited. Notably, the roughness convergence rate of EHM was fast. The surface was rapidly smoothed from 0.26 to 0.1 nm Sq after 1 h of polishing. After processing for 2 h, the roughness was further reduced to 0.09 nm. Finally, it continued to decrease and stabilized at approximately 0.06 nm. Thus, these results demonstrate that EHM can efficiently achieve an atomically smooth surface. This is because the enzyme promotes the hydrolysis reaction and promptly refreshes the active sites of the polymer pad, thereby greatly increasing the polishing rate. The Sq roughness and AFM image of the as-received Si substrate are displayed in Fig. 8(e). The Sq roughness was 0.54 nm in 5 μm × 5 μm area. Some microscratches were observed in the AFM image, which was processed via commercial CMP. As depicted in Fig. 8(f), a surface with atomic-level smoothness (0.05 nm Sq) was achieved via EHM. As shown in the AFM images, any microscopic scratches or pits cannot be found on the EHM processed surface. The data in Fig. S3 in Appendix A further demonstrate the stability and reliability of EHM.

3.5.2. Subsurface analysis

In terms of the chemical reaction mechanism, EHM does not introduce any subsurface damage. We investigated the subsurface features of the Si (100) substrate before and after EHM processing. Cross-sectional images of the Si (with and without EHM treatment) were acquired using TEM. We deposited a multi-layer protective coating (carbon layer plus Pt layers) on the surface to protect against FIB-induced damage in the course of sample preparation.

The cross-section of the initial Si substrate is shown in Fig. 8(g). As depicted, a rough surface can be seen at the interface because of the use of mechanical abrasives and chemical oxidants. As shown in Fig. 8(g), the as-received surface was not very flat, which was consistent with the AFM measurements.

In contrast, the surface presented an atomically smooth feature after being processed by EHM. As presented in Fig. 8(h), the interface was highly flat, with no detectable cracks or dislocations over a range of several micrometers. The corresponding inset displays a clear selected area electron diffraction (SAED) pattern, which confirms that the sample has high crystalline quality without any damage or deformation. Magnified views of the interface are shown in Fig. 8(h). The presence of a regular crystalline structure at the interface confirmed the elimination of the amorphous layer. Notably, the interface was smooth and geometrically highly ordered without missing or extra Si atoms. Thus, EHM is an atomic-scale machining method that is crystallographically perfect.

Journal Pre-proofs

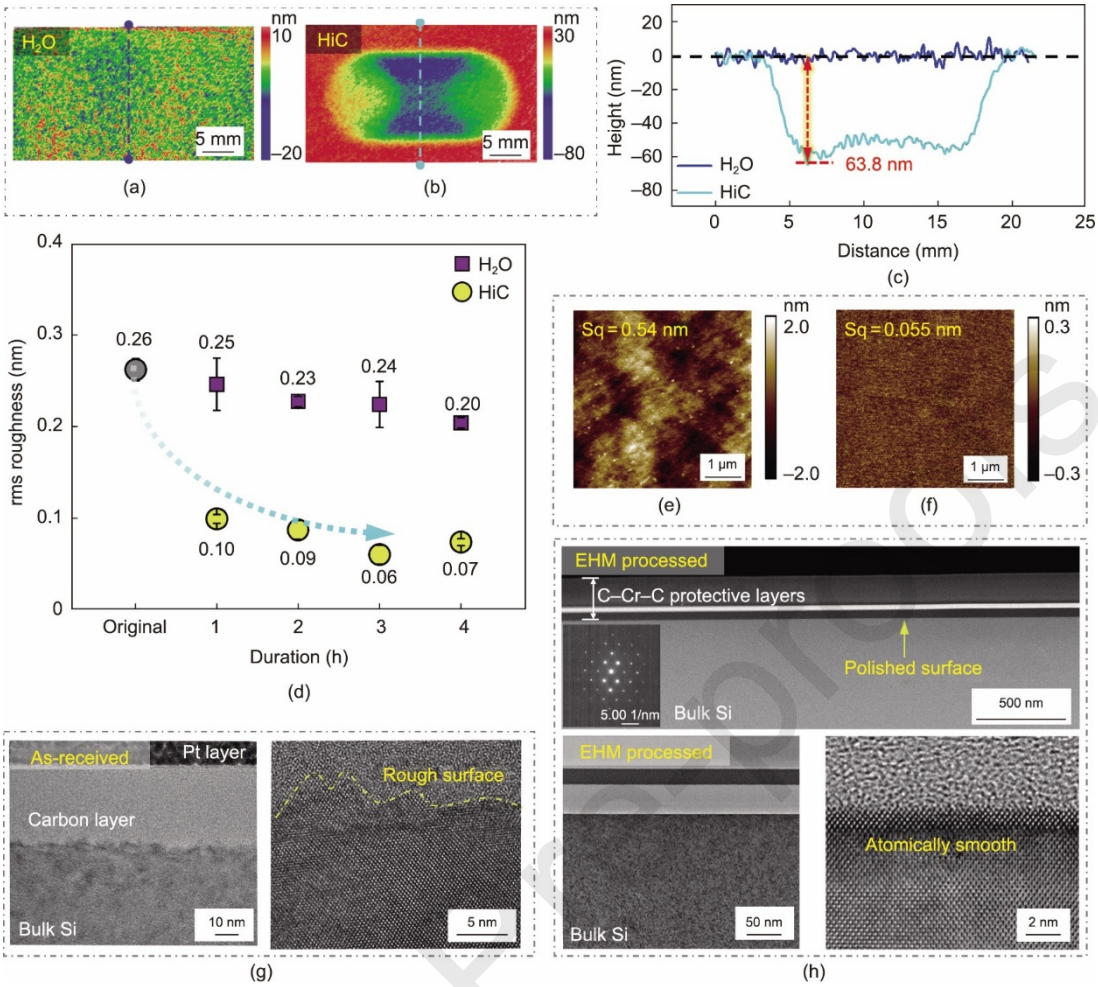

Fig. 8. (a, b) Removal patterns and profiles of Si in pure water and HiC enzyme solution. (c) Removal depths of Si in pure water and HiC enzyme solution. (d) Roughness evolution of Si processing in pure water and the HiC enzyme. (e, f) AFM images and roughness of the (e) as-received Si and that smoothed via the (f) HiC enzyme. (g) TEM images of as-received Si. (h) TEM images of the EHM-processed surface at different magnifications. The SAED pattern of the EHM-processed surface is shown in inset.

3.5.3. EHM for SiO_2, 4H-SiC, and GaN

To verify the versatility of EHM, it was applied to several typical optical and semiconductor materials, such as fused quartz (SiO_2), single-crystal 4H-SiC, and GaN. Characterized by chemical inertness and high hardness, these materials are typically hard to machine. The hardness, chemical energy, and other mechanical and chemical properties clearly differ from those of Si. For example, 4H-SiC owns extremely high hardness, surpassed only by diamond. It is difficult to obtain perfect surfaces with low surface roughness without scratches or subsurface damage. The size of the SiO_2 substrate was 40 mm × 40 mm, whereas it was 10 mm × 10 mm for the 4H-SiC and GaN substrates.

Notably, EHM for polishing is not sensitive to these parameters. The polishing experiments were carried out for SiO_2, 4H-SiC, and GaN under the same parameters. Line scanning with a step of 20 mm was utilized. The loading force was 5 N, and the rotation speed was 200 r·min^{-1}. The polishing duration was 2 h.

As shown in Fig. 9, for the fused quartz SiO_2, the Sq roughness before polishing was 0.19 nm. After EHM smoothing for 2 h, the Sq surface roughness was reduced to 0.069 nm. Thus, an atomically smooth surface can also be achieved on the SiO_2 surface via EHM. Given the relatively high ionicity of the Si–O bond, the EHM process is projected to have greater applicability to SiO_2 substrates. For 4H-SiC, the initial Sq roughness was 0.51 nm. Notably, the surface was smoothed to an atomic level of 0.059 nm Sq. With respect to the GaN material, many micropits were observed in the as-received AFM image. The initial roughness was 0.31 nm Sq. It was reduced to 0.087 nm after being processed by EHM. The results presented in Fig. 9 demonstrate that EHM serves as a universal method for polishing typical optical and semiconductor materials.

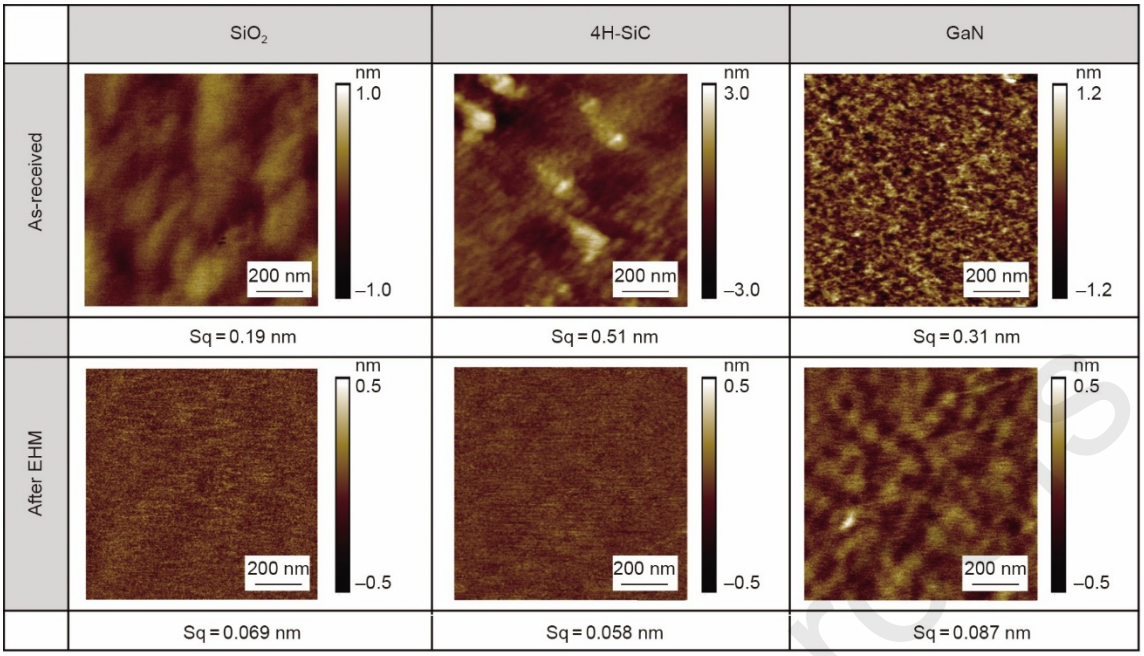

Fig. 9. Application of EHM for SiO_2, 4H-SiC, and GaN. AFM topographies and roughness of the as-received surfaces and polished surfaces via EHM.

3.6. Application for Si mirrors

In practical industrial production, the global smoothness of the mirror surface is crucial. For advanced X-ray sources, it is required that the Si mirror possess a surface roughness below 0.1 nm to enhance the reflectivity. EHM is simple and cost-effective, with only enzyme solutions and polymer tools employed, making it very convenient to apply to large mirrors.

As shown in Fig. 10(a), we used a robot to carry out the experiment. This robot controlled the motion path, loading force, and rotation of the polishing pad. Damping cloth pads and HiC enzymes were used for the experiments. The pad had a diameter of 30 mm. An image of the Si planar mirror with a size of 100 mm × 50 mm × 10 mm is displayed in Fig. 10(b). The raster scanning path with a 1 $mm \cdot s^{-1}$ feed rate was employed for polishing as the inset shown. The step pitch was 1 mm. The loading force was 5 N, and the polishing duration was 8 h. The rotation speed was 100 $r \cdot min^{-1}$. As presented in Fig. 10(c), the original Sq roughness was 0.32 nm in the 1 μm × 1 μm area. After being processed by EHM, an atomically smooth surface (0.062 nm Sq roughness) was obtained as depicted in Fig. 10(d). We measured many sites on the entire surface. The roughness was distributed uniformly after EHM, and all the values were less than 0.1 nm. The form accuracy before polishing is shown in Fig. 10(e). The PV (RMS) was 906.7 nm (206.4 nm). After IBF, the form error RMS was reduced to 2.03 nm, as shown in Fig. 10(f). After EHM for 8 h, the form error RMS increased to 3.49 nm, as shown in Fig. 10(g). The removal mark can be clearly seen, and the removal depth was approximately 12 nm. The results showed that EHM did not significantly deteriorate the surface form accuracy owing to its low MRR. The impact on the form accuracy can be further improved by optimizing the polishing duration and scan path. Therefore, numerically controlled EHM can achieve entire surface atomic-level smoothing.

Journal Pre-proofs

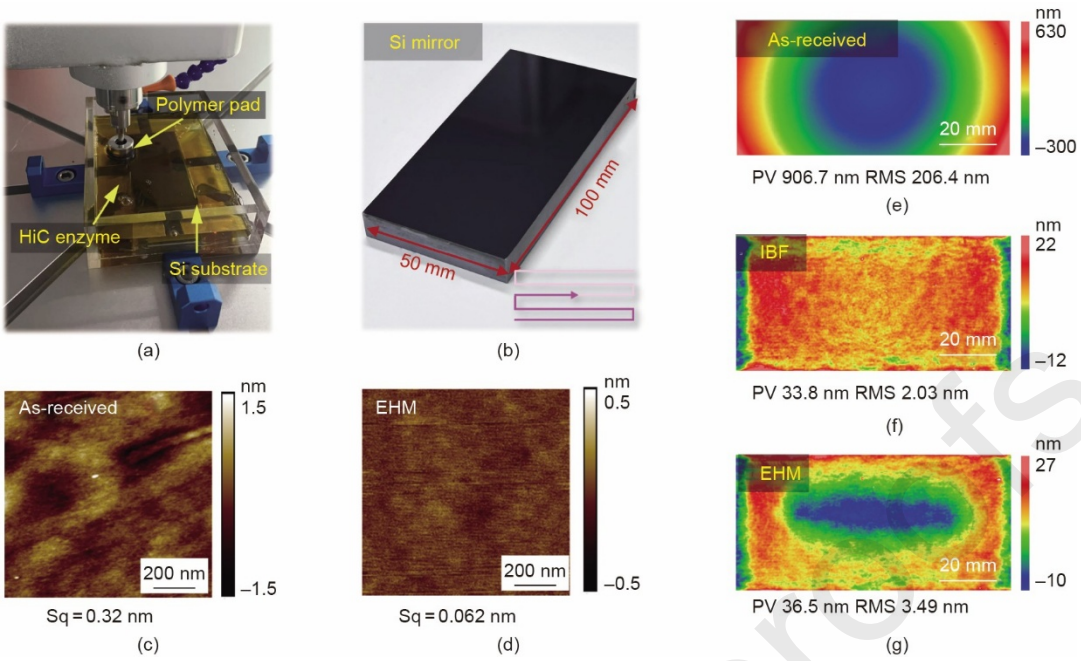

Fig. 10. Application of EHM for Si mirrors. (a) Photograph of EHM processing of a Si mirror. (b) Photograph of the Si mirror. Surface roughness (c) before and (d) after EHM. Surface form errors of the (e) material as-received, (f) after IBF, and (g) after EHM.

4. Conclusions

In this paper, we studied the EHM process as a promising atomic-scale machining technique. EHM is based on the enzymatic hydrolysis and dehydration reactions, which eventually result in atomic-scale material removal and an atomically smooth surface. The enzymatic hydrolysis phenomenon, material removal capabilities, and atomic-level smoothing characteristics have been presented.

(1) Compared with pure water, enzymes used as biocatalysts greatly increase the hydrolysis rate of polymers, thereby generating a large number of reactive groups. Static incubation experiments and FTIR analysis revealed that the ester bonds are efficiently cleaved in the enzyme solution.

(2) Si atoms are removed through the hydrolysis reaction and dehydration reaction with the formation of Si–O–C bridge bonds. The removal depth via EHM was 13 times greater than that in pure water. EHM achieved deterministic material removal at the atomic scale with a VRR of 3.8×10^{-5} $mm^3 \cdot min^{-1}$.

(3) EHM is a generic approach for different materials. Atomically smooth surfaces with sub-0.1 nm Sq roughness were achieved for Si, SiO_2, SiC, and GaN. The smooth surface had high surface integrity and crystalline quality. Full-surface smoothing was accomplished through the combination of numerically controlled scanning.

(4) EHM offers broad applicability for enzymes (RoL, CALB, and HiC, etc.), polymer materials (PBS, PCL, and PU, etc.), and workpiece materials.

In the long term, we investigate the ability of the EHM to correct low- and mid-spatial-frequency errors. EHM offers a novel strategy for the processing of optical and semiconductor materials, and it holds profound significance for advancing atomic-scale manufacturing [57].

Appendix A. Supporting Information

Journal Pre-proofs

CRediT authorship contribution statement

Bing Wu: Data curation, Conceptualization, Methodology, Writing – original draft. **Yongjie Zhang:** Methodology, Validation, Writing – review & editing. **Yinhui Wang:** Investigation, Writing – review & editing. **Yongyu Fan:** Methodology. **Rongyan Sun:** Supervision, Writing – review & editing. **Hui Deng:** Funding acquisition, Conceptualization, Supervision, Writing – review & editing.

Declaration of competing interest

The authors declare that they have no known competing financial interests or personal relationships that could have appeared to influence the work reported in this paper.

Acknowledgements

This work is financially supported by the research fund from the National Natural Science Foundation of China (52450164 and 52505488), the Guangdong Basic and Applied Basic Research Foundation (2024B1515020027 and 23201910240001664), the Science, Technology and Innovation Commission of Shenzhen Municipality (GJHZ20240218111401003), the Shenzhen Engineering Research Center for Semiconductor-specific Equipment (XMHT20230111003), and the China Postdoctoral Science Foundation under Grant Number 2025M771393. The authors acknowledge the assistance of SUSTech Core Research Facilities.

References

[1] Mimura H, Handa S, Kimura T, Yumoto H, Yamakawa D, Yokoyama H, et al. Breaking the 10 nm barrier in hard-X-ray focusing. Nat Phys 2010;6(2):122–5.

[2] Wagner C, Harned N. Lithography gets extreme. Nat Photonics 2010;4(1):24–6.

[3] Savage D, Kleiner J, Schimke N, Phang YH, Jankowski T, Jacobs J, et al. Determination of roughness correlations in multilayer films for X-ray mirrors. J Appl Phys 1991;69(3):1411–24.

[4] Wang T, Huang L, Zhu Y, Giorgio S, Boccabella P, Bouet N, et al. Ion beam figuring system for synchrotron X-ray mirrors achieving sub-0.2-μrad and sub-0.5-nm root mean square. Nanomanuf Metrol 2023;6(1):20.

[5] Goswami S, Slinker K, Friesen M, McGuire L, Truitt J, Tahan C, et al. Controllable valley splitting in silicon quantum devices. Nat Phys 2007;3(1):41–5.

[6] Mori Y, Yamauchi K, Endo K. Elastic emission machining. Precis Eng 1987;9(3):123–8.

[7] Liu H, Zhang J, Jiang Q, Zhang B. Material removal mechanisms in ultra-high-speed machining. Engineering 2025;55:51–70.

[8] Cui M, Lu L, Zhang Z, Guan Y. A laser scanner-stage synchronized system supporting the large-area precision polishing of additive-manufactured metallic surfaces. Engineering 2021;7(12):1732–40.

[9] Weiser M. Ion beam figuring for lithography optics. Nucl Instrum Methods Phys Res Sect B 2009;267(8–9):1390–3.

[10] Yamauchi K, Mimura H, Inagaki K, Mori Y. Figuring with subnanometer-level accuracy by numerically controlled elastic emission machining. Rev Sci Instrum 2002;73(11):4028–33.

[11] Arnold T, Pietag F. Ion beam figuring machine for ultra-precision silicon spheres correction. Precis Eng 2015;41:119–25.

[12] Zhou L, Dai Y, Xie X, Li S. Optimum removal in ion-beam figuring. Precis Eng 2010;34(3):474–9.

[13] Sigmund P. Sputtering by ion bombardment theoretical concepts. In: Behrisch R, editor. Sputtering by particle bombardment I. Berlin: Springer; 2005. p. 9–71.

[14] Mori Y, Yamauchi K, Endo K. Mechanism of atomic removal in elastic emission machining. Precis Eng 1988;10(1):24–8.

Journal Pre-proofs

[15] Katoh J, Arima K, Kubota A, Mimura H, Inagaki K, Mori Y, et al. Atomic-scale evaluation of Si (111) surfaces finished by the planarization process utilizing SiO_2 particles mixed with water. J Electrochem Soc 2006;153(6):G560.

[16] Mimura H, Yumoto H, Matsuyama S, Yamamura K, Sano Y, Endo K, et al. Surface figuring and measurement methods with spatial resolution close to 0.1 mm for X-ray mirror fabrication. In: Proceedings of the Advances in Metrology for X-Ray and EUV Optics; 2005 Jul 31–Aug 4; San Diego, CA, USA. Bellingham: SPIE; 2005. p. 59210M.

[17] Yumoto H, Mimura H, Koyama T, Matsuyama S, Tono K, Togashi T, et al. Focusing of X-ray free-electron laser pulses with reflective optics. Nat Photonics 2013;7(1):43–7.

[18] Zhao F, Zhang Z, Deng X, Feng J, Zhou H, Liu Z, et al. Atomic surface achieved through a novel cross-scale model from macroscale to nanoscale. Nanoscale 2024;16(5):2318–36.

[19] Dong L, Zhang Z, Zhao F, Li Q, Zhou H, Yang X, et al. Atomic surface on a Ni alloy produced by novel green chemical mechanical polishing. Tribol Int 2025;211:110902.

[20] Gu Q, Zhang Z, Zhou H, Yu J, Wang D, Feng J, et al. A novel approach of jet polishing for interior surface of small-grooved components using three developed setups. Int J Extreme Manuf 2024;6(2):025101.

[21] Yu Z, Zhang Z, Zeng Z, Fan C, Gu Y, Shi C, et al. Atomic surface of diamond induced by novel green photocatalytic chemical mechanical polishing with high material removal rate. Int J Extreme Manuf 2025;7(2):025102.

[22] Cui X, Zhang Z, Yu S, Chen X, Shi C, Zhou H, et al. Unprecedented atomic surface of silicon induced by environmentally friendly chemical mechanical polishing. Nanoscale 2023;15(21):9304–14.

[23] Zhao F, Zhang Z, Zhou H, Chen L, Hai K, Wu L, et al. Unprecedented developed composite polishing system to achieve atomic surface integrating rough and fine polishing using a novel hyper-conjugated pad through controlling the temperature of a proposed green slurry. Adv Compos Hybrid Mater 2025;8:234.

[24] Okamoto T, Sano Y, Tachibana K, Arima K, Hattori AN, Yagi K, et al. Dependence of process characteristics on atomic-step density in catalyst-referred etching of 4H-SiC(0001) surface. J Nanosci Nanotechnol 2011;11(4):2928–30.

[25] Hara H, Sano Y, Mimura H, Arima K, Kubota A, Yagi K, et al. Novel abrasive-free planarization of 4H-SiC (0001) using catalyst. J Electron Mater 2006;35(8):L11–4.

[26] Isohashi A, Bui PV, Toh D, Matsuyama S, Sano Y, Inagaki K, et al. Chemical etching of silicon carbide in pure water by using platinum catalyst. Appl Phys Lett 2017;110(20):201601.

[27] Bui P, Isohashi A, Kizaki H, Sano Y, Yamauchi K, Morikawa Y, et al. Study on the mechanism of platinum-assisted hydrofluoric acid etching of SiC using density functional theory calculations. Appl Phys Lett 2015;107(20):201601.

[28] Bui PV, Sano Y, Morikawa Y, Yamauchi K. Characteristics and mechanism of catalyst-referred etching method: application to 4H-SiC. Int J Automot Technol 2018;12(2):154–9.

[29] Toh D, Bui PV, Isohashi A, Matsuyama S, Yamauchi K, Sano Y. An abrasive-free chemical polishing method assisted by nickel catalyst generated by *in situ* electrochemical plating. Rev Sci Instrum 2020;91(4):045108.

[30] Toh D, Kayao K, Bui PV, Inagaki K, Morikawa Y, Yamauchi K, et al. Catalyst enhancement approach for improving the removal rate and stability of silica glass polishing via catalyzed chemical etching in pure water. Precis Eng 2023;84:21–7.

[31] Gunaydin H, Houk KN. Molecular dynamics prediction of the mechanism of ester hydrolysis in water. J Am Chem Soc 2008;130(46):15232–3.

[32] Yates K, McClelland RA. Mechanisms of ester hydrolysis in aqueous sulfuric acids. J Am Chem Soc 1967;89(11):2686–92.

[33] Guo J, Matsuzawa Y, Yamaguchi G, Mimura H. Atomic-level smoothing of glass and silicon surfaces by water polishing with an acrylic polymer plate. Appl Phys Lett 2022;120(9):094105.

[34] Guo J, Egawa S, Motoyama H, Mimura H. Study on chemical mechanism of processing silicon by PMMA in water. J Appl Phys 2025;137(1):015303.

[35] Egawa S, Matsuzawa Y, Hiraguri K, Motoyama H, Yamaguchi G, Yokomae S, et al. Figure correction of a Wolter mirror master mandrel by organic abrasive machining. Rev Sci Instrum 2023;94(5):053707.

[36] Matsuzawa Y, Hiraguri K, Hashizume H, Mimura H. Organic abrasive machining system for optical fabrication with 0.1-mm spatial resolution. Rev Sci Instrum 2022;93(1):013101.

Journal Pre-proofs

[37] Hoshino A, Isono Y. Degradation of aliphatic polyester films by commercially available lipases with special reference to rapid and complete degradation of poly(L-lactide) film by lipase PL derived from Alcaligenes sp. Biodegradation 2002;13(2):141–7.

[38] Lim HA, Raku T, Tokiwa Y. Hydrolysis of polyesters by serine proteases. Biotechnol Lett 2005;27(7):459–64.

[39] Bai Z, Shi K, Su T, Wang Z. Correlation between the chemical structure and enzymatic hydrolysis of Poly (butylene succinate), Poly (butylene adipate), and Poly (butylene suberate). Polym Degrad Stabil 2018;158:111–8.

[40] Rosato A, Romano A, Totaro G, Celli A, Fava F, Zanaroli G, et al. Enzymatic degradation of the most common aliphatic bio-polyesters and evaluation of the mechanisms involved: an extended study. Polymers 2022;14(9):1850.

[41] Zumstein MT, Rechsteiner D, Roduner N, Perz V, Ribitsch D, Guebitz GM, et al. Enzymatic hydrolysis of polyester thin films at the nanoscale: effects of polyester structure and enzyme active-site accessibility. Environ Sci Technol 2017;51(13):7476–85.

[42] Di Bisceglie F, Quartinello F, Vielnascher R, Guebitz GM, Pellis A. Cutinase-catalyzed polyester-polyurethane degradation: elucidation of the hydrolysis mechanism. Polymers 2022;14(3):411.

[43] Almeida BC, Figueiredo P, Carvalho AT. Polycaprolactone enzymatic hydrolysis: a mechanistic study. ACS Omega 2019;4(4):6769–74.

[44] Yoshiyuki U. KANEEDA T, YOKOMIZO S. Bio-machining of metals by bacteria Thiobacillus ferrooxidans. In: Proceedings of the 7th International Precision Engineering Seminar; 1993 May; Kobe, Japan. Amsterdam: Elsevier; 1993. p. 290–301.

[45] Díaz-Tena E, Gallastegui G, Hipperdinger M, Donati ER, Ramírez M, Rodríguez A, et al. New advances in copper biomachining by iron-oxidizing bacteria. Corros Sci 2016;112:385–92.

[46] Díaz-Tena E, Barona A, Gallastegui G, Rodríguez A, López de Lacalle LN, Elías A. Biomachining: metal etching via microorganisms. Crit Rev Biotechnol 2017;37(3):323–32.

[47] Santaolalla A, Alvarez-Braña Y, Barona A, Basabe-Desmonts L, Benito-Lopez F, Rojo N. Sustainable mold biomachining for the manufacturing of microfluidic devices. J Ind Eng Chem 2023;120:332–9.

[48] Eskandarian M, Karimi A, Shabgard M. Studies on enzymatic biomachining of copper by glucose oxidase. J Taiwan Inst Chem Eng 2013;44(2):331–5.

[49] Ma F, Zheng M, Huang H, San Y, Xiong W, Yang Y. Application research status and prospect of biomachining in the manufacturing. Int J Adv Manuf Technol 2025;139(1-2):1–13.

[50] Meenarathi B, Chen HH, Chen PH, Anbarasan R. Synthesis and characterization of fluorescent bio-degradable poly(ε-caprolactone). Int J Plast Technol 2014;18(1):135–45.

[51] Parthasarathy V, Sundaresan B, Dhanalakshmi V, Anbarasan R. Melt surface grafting of HDPE with mercaptoesters by thermolysis method. Polym Eng Sci 2010;50(3):474–83.

[52] Åkerlund E, Diez-Escudero A, Grzeszczak A, Persson C. The effect of PCL addition on 3D-printable PLA/HA composite filaments for the treatment of bone defects. Polymers 2022;14(16):3305.

[53] Liu B, Guan T, Wu G, Fu Y, Weng Y. Biodegradation behavior of degradable mulch with poly(butylene adipate-co-terephthalate) (PBAT) and poly(butylene succinate) (PBS) in simulation marine environment. Polymers 2022;14(8):1515.

[54] Tang L, Su C, Chen Y, Xian Y, Hui X, Ye Z, et al. Influence of biodegradable polybutylene succinate and non-biodegradable polyvinyl chloride microplastics on anammox sludge: performance evaluation, suppression effect and metagenomic analysis. J Hazard Mater 2021;401:123337.

[55] Kaur A, Chahal P, Hogan T. Selective fabrication of SiC/Si diodes by excimer laser under ambient conditions. IEEE Electron Device Lett 2016;37(2):142–5.

[56] Toh D, Bui PV, Isohashi A, Kidani N, Matsuyama S, Sano Y, et al. Catalyzed chemical polishing of SiO_2 glasses in pure water. Rev Sci Instrum 2019;90(4):045115.

[57] Fang F. Atomic and close-to-atomic scale manufacturing: perspectives and measures. Int J Extreme Manuf 2020;2(3):030201.

Journal Pre-proofs

Declaration of interests

☒ The authors declare that they have no known competing financial interests or personal relationships that could have appeared to influence the work reported in this paper.

☐The authors declare the following financial interests/personal relationships which may be considered as potential competing interests:

Journal Pre-proofs